E. Wolf, Progress in Optics 50

Chapter 2

Conical diffraction: Hamilton's diabolical point at the heart of crystal optics

by

M.V. Berry, M.R. Jeffrey

H.H. Wills Physics Laboratory, Tyndall Avenue, Bristol BS8 1TL, UK

ISSN: 0079-6638 DOI: 10.1016/S0079-6638(07)50002-8

Contents

§ 1. Introduction

The bicentenary of the birth in 1805 of William Rowan Hamilton (fig. 1) comes at a time of renewed interest in the phenomenon of conical refraction (Born and Wolf [1999], Landau, Lifshitz and Pitaevskii [1984]), in which a narrow beam of light, incident along the optic axis of a biaxial crystal, spreads into a hollow cone within the crystal, and emerges as a hollow cylinder. The prediction of the effect in 1832 (Hamilton [1837]), and its observation by Lloyd (fig. 1) soon afterwards (Lloyd [1837]), caused a sensation. For a non-technical account, see Lunney and Weaire [2006].

Our purpose here is to describe how the current understanding of conical refraction has been reached after nearly two centuries of theoretical and experimental study. Although our treatment will be roughly historical, we do not adhere to the practice, common in historical research, of describing each episode using only sources and arguments from the period being studied. For the early history of conical refraction, this has already been done, by Graves [1882] and O'Hara [1982]. Rather, we will weave each aspect of the theory into the historical development in ways more concordant with the current style of theoretical physics, hoping thus to bring out connections with other phenomena in mathematics and physics.

There are many reasons why conical refraction is worth revisiting:

(i) It was an early (perhaps the first) example of a qualitatively new phenomenon predicted by mathematical reasoning. By the early 1800s, it was widely appreciated that mathematics is essential to understanding the natural world. However, the phenomena to which mathematics had been applied were already familiar (e.g., tides, eclipses, and planetary orbits). Prediction of qualitatively new effects by mathematics may be commonplace today, but in the 1830s it was startling.

(ii) With its intimate interplay of position and direction, conical refraction was the first non-trivial application of phase space, and of what we now call dynamics governed by a Hamiltonian.

(iii) Its observation provided powerful evidence confirming that light is a transverse wave.

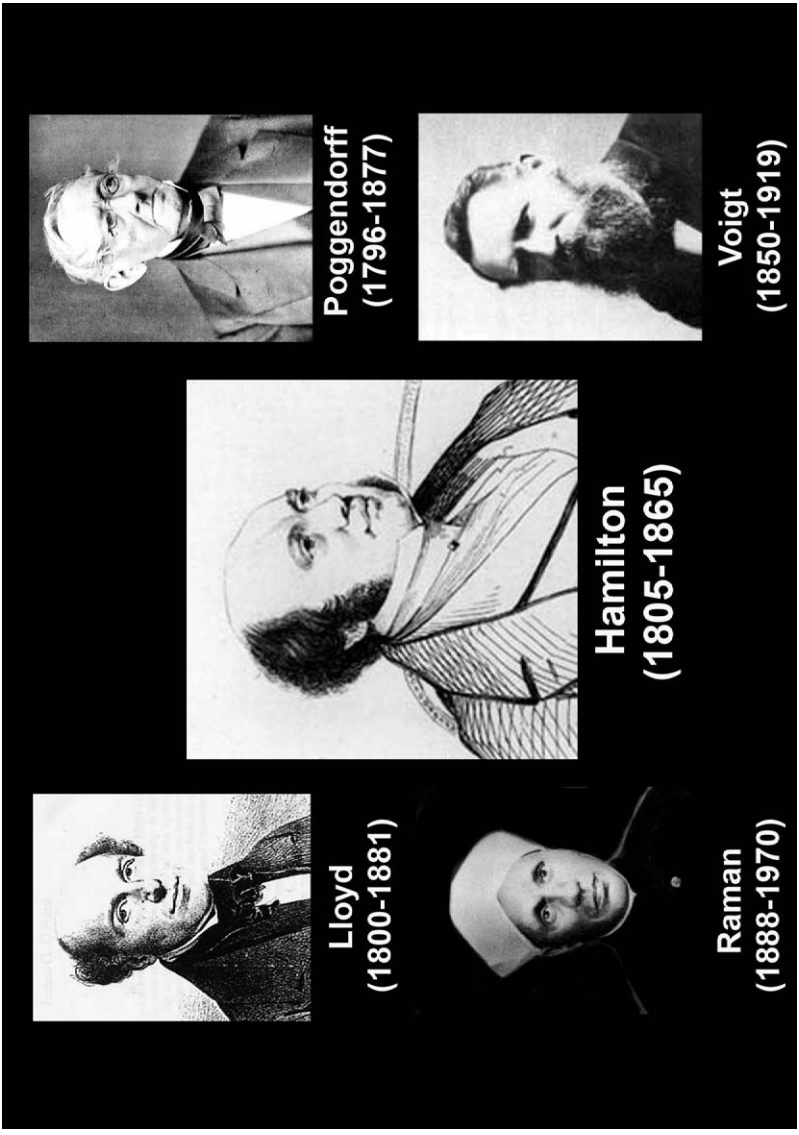

Fig. 1. Dramatis personae.

(iv) Recently, it has become popular to study light through its singularities (Berry [2001], Nye [1999], Soskin and Vasnetsov [2001]). In retrospect, we see conical refraction as one of the first phenomena in singular polarization optics; another is the pattern of polarization in the blue sky (Berry, Dennis and Lee [2004]).

(v) It was the first physical example of a conical intersection (diabolical point) (Berry [1983], Uhlenbeck [1976], Berry and Wilkinson [1984]) involving a degeneracy. Nowadays, conical intersections are popular in theoretical chemistry, as spectral features indicating the breakdown of the Born–Oppenheimer separation between fast electronic and slow nuclear freedoms (Cederbaum, Friedman, Ryaboy and Moiseyev [2003], Herzberg and Longuet-Higgins [1963], Mead and Truhlar [1979]). By analogy, conical refraction can be reinterpreted as an exactly solvable model for quantum physics in the presence of a degeneracy.

(vi) The effect displays a subtle interplay of ray and wave physics. Although its original prediction was geometrical (Sections 3 and 4), there are several levels of geometrical optics (Sections 5 and 7), of which all except the first require concepts from wave physics, and waves are essential to a detailed understanding (Section 6). That is why we use the term conical diffraction, and why the effect has taken so long to understand.

(vii) Analysis of the theory (Berry [2004b]) led to identification of an unexpected universal phenomenon in mathematical asymptotics: when exponential contributions to a function compete, the smaller exponential can dominate (Berry [2004a]).

(viii) There are extensions (Section 8) of the case studied by Hamilton, and their theoretical understanding still presents challenges. Effects of chirality (optical activity) have only recently been fully understood (Belsky and Stepanov [2002], Berry and Jeffrey [2006a]), and further extensions incorporate absorption (Berry and Jeffrey [2006b], Jeffrey [2007]) and nonlinearity (Indik and Newell [2006]).

(ix) Conical diffraction is a continuing stimulus for experiments. Although the fine details of Hamilton's original phenomenon have now been observed (Berry, Jeffrey and Lunney [2006]), predictions of new structures that appear in the presence of chirality, absorption and nonlinearity remain untested.

(x) The story of conical diffraction, unfolding over 175 years, provides an edifying contrast to the current emphasis on short-term science.

Although all results of the theory have been published before, some of our ways of presenting them are original. In particular, after the exact treatment in

Sections 2–4 we make systematic use of the simplifying approximation of paraxiality. This is justified by the small angles involved in conical diffraction (Appendix 1), and leads to what we hope are the simplest quantitative explanations of the various phenomena.

§ 2. Preliminaries: electromagnetism and the wave surface

Hamilton's prediction was based on a singular property of the wave surface describing propagation in an anisotropic medium. Originally, this was formulated in terms of Fresnel's elastic-solid theory. Today it is natural to use Maxwell's electromagnetic theory.

For the physical fields in a homogeneous medium, we write plane waves with wavevector $\mathbf{k}$ and frequency ω as

$$\mathrm{Re}\big[\{\mathbf{D_k}, \mathbf{E_k}, \mathbf{B_k}, \mathbf{H_k}\} \exp\big\{\mathrm{i}(\mathbf{k}\cdot\mathbf{r} - \omega t)\big\}\big], \tag{2.1}$$

in which the vectors $\mathbf{D_k}$, etc., are usually complex. From Maxwell's curl equations,

$$\omega\mathbf{D_k} = -\mathbf{k}\times\mathbf{H_k}, \qquad \omega\mathbf{B_k} = \mathbf{k}\times\mathbf{E_k}. \tag{2.2}$$

A complete specification of the fields requires constitutive equations. For a transparent nonmagnetic nonchiral biaxial dielectric, these can be written as

$$\mathbf{E_k} = \boldsymbol{\varepsilon}^{-1}\mathbf{D_k}, \qquad \mathbf{B_k} = \mu_0\mathbf{H_k}. \tag{2.3}$$

$\boldsymbol{\varepsilon}^{-1}$ is the inverse dielectric tensor, conveniently expressed in principal axes as

$$\boldsymbol{\varepsilon}^{-1} = \frac{1}{\varepsilon_0}\begin{pmatrix} 1/n_1^2 & 0 & 0 \\ 0 & 1/n_2^2 & 0 \\ 0 & 0 & 1/n_3^2 \end{pmatrix}, \tag{2.4}$$

where n_i are the principal refractive indices, all different, with the conventional ordering

$$n_1 < n_2 < n_3. \tag{2.5}$$

For biaxiality (all n_i different), the microscopic structure of the material must have sufficiently low symmetry; in the case of crystals, this is a restriction to the orthorhombic, monoclinic or triclinic classes (Born and Wolf [1999]). Conical refraction depends on the differences between the indices, so we define

$$\alpha \equiv \frac{1}{n_1^2} - \frac{1}{n_2^2}, \qquad \beta \equiv \frac{1}{n_2^2} - \frac{1}{n_3^2}. \tag{2.6}$$

It will be convenient to express the wavevector $\mathbf{k}$ in terms of the refractive index $n_{\mathbf{k}}$, through the definitions

$$\mathbf{k} \equiv k\mathbf{e}_{\mathbf{k}} \equiv k_0 n_{\mathbf{k}} \mathbf{e}_{\mathbf{k}}, \quad k_0 \equiv \frac{\omega}{c}, \tag{2.7}$$

incorporating

$$c = \frac{1}{\sqrt{\varepsilon_0 \mu_0}}. \tag{2.8}$$

It is simpler to work with the electric vector $\mathbf{D}$ rather than $\mathbf{E}$, because $\mathbf{D}$ is always transverse to the propagation direction $\mathbf{e}_{\mathbf{k}}$. Then eqs. (2.2) and (2.3) lead to the following eigenequation determining the possible plane waves:

$$\frac{1}{n_{\mathbf{k}}^2} \mathbf{D}_{\mathbf{k}} = -\mathbf{e}_{\mathbf{k}} \times \mathbf{e}_{\mathbf{k}} \times \left(\varepsilon_0 \boldsymbol{\varepsilon}^{-1} \cdot \mathbf{D}_{\mathbf{k}}\right). \tag{2.9}$$

This involves a 3×3 matrix whose determinant vanishes, and the two eigenvalues $\lambda_\pm$ of the 2×2 inverse dielectric tensor transverse to $\mathbf{k}$ give the refractive indices

$$n_{\mathbf{k}\pm} = \frac{1}{\sqrt{\lambda_\pm(\mathbf{e}_{\mathbf{k}})}}. \tag{2.10}$$

Of several different graphical representations (Born and Wolf [1999], Landau, Lifshitz and Pitaevskii [1984]) of the propagation governed by $n_{\mathbf{k}\pm}$, we choose the two-sheeted polar plot in direction space; this is commonly called the wave surface, though there is no universally established terminology. The wave surface has the same shape as the constant ω surface in $\mathbf{k}$ space, that is [cf. eq. (2.7)], the contour surface of the dispersion relation

$$\omega(\mathbf{k}) \equiv \frac{ck}{n_{\mathbf{k}}}; \tag{2.11}$$

$\omega(\mathbf{k})$ is the Hamiltonian generating rays in the crystal, with $\mathbf{k}$ as canonical momentum.

An immediate application of the wave surface, known to Hamilton and central to his discovery, is that for each of the two waves with wavevector $\mathbf{k}$, the ray direction, that is, the direction of energy transport, is perpendicular to the corresponding sheet of the surface. This can be seen from the first Hamilton equation, according to which the group (ray) velocity is

$$\mathbf{v}_{\mathrm{g}} = \nabla_{\mathbf{k}} \omega(\mathbf{k}) \tag{2.12}$$

(for this case of a homogeneous medium, the second Hamilton equation simply asserts that $\mathbf{k}$ is constant along a ray). Alternatively (Landau, Lifshitz and

Pitaevskii [1984]), the ray direction can be regarded as that of the Poynting vector,

$$\mathbf{S} = \mathrm{Re}\,\mathbf{E}^* \times \mathbf{H}, \tag{2.13}$$

because for any displacement d$\mathbf{k}$ with ω constant – that is, any displacement in the wave surface –

$$\mathbf{S} \cdot \mathrm{d}\mathbf{k} = \frac{1}{2}\omega\,\mathrm{Re}\big[\mathbf{E}^* \cdot \mathrm{d}\mathbf{D} - \mathrm{d}\mathbf{E}^* \cdot \mathbf{D} + \mathbf{H} \cdot \mathrm{d}\mathbf{B}^* - \mathrm{d}\mathbf{H} \cdot \mathbf{B}^*\big] = 0, \tag{2.14}$$

where the first equality is a consequence of Maxwell's equations and the second follows from the linearity and Hermiticity of the constitutive relations (2.3). (This argument is slightly more general than that of Landau, Lifshitz and Pitaevskii [1984], because it includes transparent media that are chiral as well as biaxial.)

§ 3. The diabolical singularity: Hamilton's ray cone

Figure 2 is a cutaway representation of the wave surface, showing four points of degeneracy where $n_{\mathbf{k}+} = n_{\mathbf{k}-}$, located on two optic axes in the k_1, k_3 plane in $\mathbf{k}$ space. Each intersection of the surfaces takes the form of a double cone, that is, a diabolo, and since these are the organizing centres of degenerate behaviour we call them diabolical points, a term adopted in quantum (Ferretti, Lami and

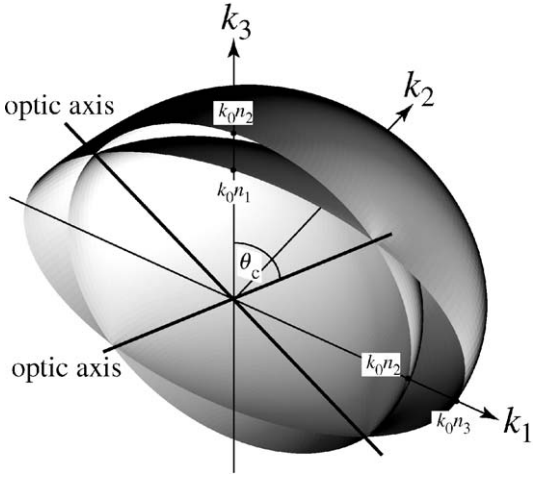

Fig. 2. Wave surface for $n_1 = 1.1$, $n_2 = 1.4$, $n_3 = 1.8$, showing the four diabolical points on the two optic axes.

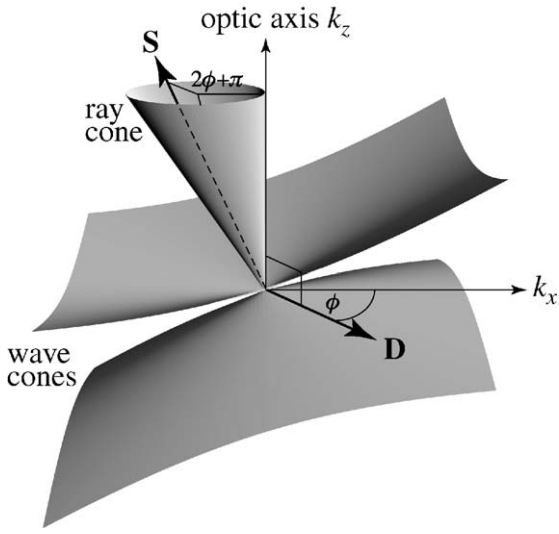

Fig. 3. The ray cone is a slant cone normal to the wave cone.

Villani [1999]) and nuclear physics (Chu, Rasmussen, Stoyer, Canto, Donangelo and Ring [1995]) as well as optics. In fact, such degeneracies are to be expected, because of the theorem of Von Neumann and Wigner [1929] that degeneracies of real symmetric matrices [such as that in (2.9)] have codimension two, and indeed we have two parameters, representing the direction of $\mathbf{k}$.

Hamilton's insight was that at a diabolical point the normals (rays) to the surfaces are not defined, so there are infinitely many normals (rays), not two as for all other $\mathbf{k}$. These normals to the wave cone define another cone. This is the ray cone (fig. 3), about whose structure – noncircular and skewed – we can learn by extending an argument of Born and Wolf [1999].

We choose $\mathbf{k}$ along an optic axis, and track the Poynting vector as $\mathbf{D}$ rotates in the plane transverse to $\mathbf{k}$. From (2.13) and Maxwell's equations, $\mathbf{S}$ can be expressed as

$$\mathbf{S} = \frac{c}{n_{\mathbf{k}}} \operatorname{Re}\big[\mathbf{E}^* \cdot \mathbf{D}\mathbf{e}_{\mathbf{k}} - \mathbf{E}^* \cdot \mathbf{e}_{\mathbf{k}}\mathbf{D}\big]. \tag{3.1}$$

Using coordinates k_x, k_y, k_z, with $\mathbf{e}_z$ along $\mathbf{k}$ and $\mathbf{e}_x$ in the k_1, k_3 plane (i.e., $\mathbf{e}_y = \mathbf{e}_2$),

$$\mathbf{D} = \begin{pmatrix} D_x \\ D_y \\ 0 \end{pmatrix}, \qquad \mathbf{E} = \begin{pmatrix} E_x \\ E_y \\ E_z \end{pmatrix} = \frac{1}{\varepsilon_0}\big(\boldsymbol{\varepsilon}'\big)^{-1}\mathbf{D}. \tag{3.2}$$

Here $\boldsymbol{\varepsilon}'$ is the rotated dielectric matrix, determined by four conditions: rotation about the y axis does not change components involving the 2 axis, the choice of $\mathbf{k}$ along an optic axis (degeneracy) implies that the xx and yy elements are the same, and the trace and determinant of the matrices $\boldsymbol{\varepsilon}$ and $\boldsymbol{\varepsilon}'$ are the same. Thus

$$\varepsilon_0\big(\boldsymbol{\varepsilon}'\big)^{-1} = \frac{1}{n_2^2}\begin{pmatrix}1&0&0\\0&1&0\\0&0&1\end{pmatrix} + \begin{pmatrix}0&0&\sqrt{\alpha\beta}\\0&0&0\\\sqrt{\alpha\beta}&0&\alpha-\beta\end{pmatrix}. \tag{3.3}$$

It follows that, in eq. (3.1),

$$\mathbf{E}^*\cdot\mathbf{D} = \frac{1}{\varepsilon_0 n_2^2}\big(|D_x|^2 + |D_y|^2\big),$$

$$E_z = \mathbf{E}^*\cdot\mathbf{e}_\mathbf{k} = \frac{1}{\varepsilon_0}\sqrt{\alpha\beta}\,D_x. \tag{3.4}$$

Denoting the direction of $\mathbf{D}$ in the k_x, k_y plane by ϕ, that is

$$D_x = D\cos\phi, \qquad D_y = D\sin\phi, \tag{3.5}$$

we obtain a ϕ-parametrized representation of the surface swept out by $\mathbf{S}$:

$$\mathbf{S} = \frac{cD^2}{\varepsilon_0 n_2^3}\left(\mathbf{e}_z - \frac{1}{2}\tan 2A(\mathbf{e}_x + \mathbf{e}_x\cos 2\phi + \mathbf{e}_y\sin 2\phi)\right). \tag{3.6}$$

This is the ray surface, in the form of a skewed noncircular cone (fig. 3), with half-angle A given by

$$\tan 2A = n_2^2\sqrt{\alpha\beta}, \tag{3.7}$$

From eq. (3.6) it is clear that in a circuit of the ray cone ($2\phi = 2\pi$), the polarization direction ϕ rotates by half a turn, illustrating the familiar 'fermionic' property of degeneracies (Berry [1984], Silverman [1980]).

The direction of the optic axis, that is, the polar angle θ_c in the xz plane (fig. 2) can be determined from the rotation required to transform $\boldsymbol{\varepsilon}$ into $\boldsymbol{\varepsilon}'$. Thus

$$\boldsymbol{\varepsilon}' = \mathbf{R}\boldsymbol{\varepsilon}\mathbf{R}^{-1}, \tag{3.8}$$

where

$$\mathbf{R} = \begin{pmatrix}\sin\theta_c&0&-\cos\theta_c\\0&1&0\\\cos\theta_c&0&\sin\theta_c\end{pmatrix}, \tag{3.9}$$

whence identification with eq. (3.3) fixes θ_c as

$$\tan\theta_c = \sqrt{\frac{\alpha}{\beta}}. \tag{3.10}$$

§ 4. The bright ring of internal conical refraction

In a leap of insight that we now recognise as squarely in the spirit of singular optics, Hamilton [1837] realised that the ray cone would appear inside a crystal slab, on which is incident a narrow beam directed along the optic axis. The hollow cone would refract into a hollow cylinder outside the slab (fig. 4). This is a singular situation because a beam incident in any other direction would emerge, doubly refracted, into just two beams, not a cylinder of infinitely many rays. This is internal conical refraction, so-called because the cone is inside the crystal.

Hamilton also envisaged external conical refraction, in which a different optical arrangement results in a cone outside the crystal. This is associated with a circle of contact between the wave surface and a tangent plane, "somewhat as a plum can be laid down on a table so as to touch and rest on the table in a whole circle of contact" (Graves [1882]). Since the theory is similar for the two effects,

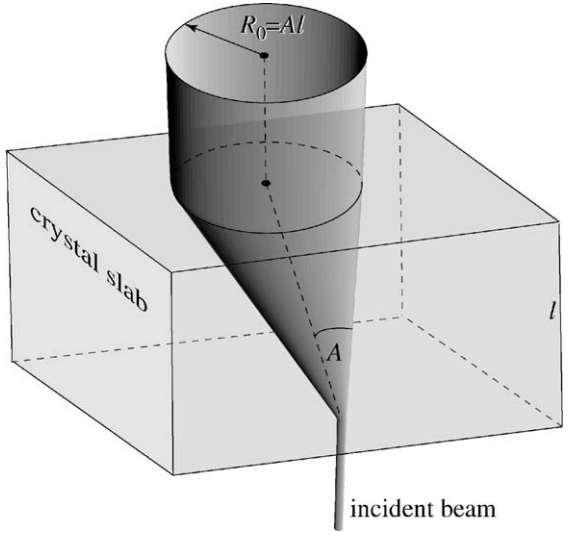

Fig. 4. Schematic of Hamilton's prediction of internal conical refraction.

our emphasis henceforth will be on internal, rather than external, conical refraction.

Hamilton's research attracted wide attention. According to Graves [1882], Airy called conical refraction "perhaps the most remarkable prediction that has ever been made"; and Herschel, in a prescient anticipation of singular optics, wrote "of theory actually remanding back experiment to read her lesson anew; informing her of facts so strange, as to appear to her impossible, and showing her all the singularities she would observe in critical cases she never dreamed of trying". In particular, the predictions fascinated Lloyd [1837], who called them "in the highest degree novel and remarkable", and regarded them as "singular and unexpected consequences of the undulatory theory, not only unsupported by any facts hitherto observed, but even opposed to all the analogies derived from experience. If confirmed by experiment, they would furnish new and almost convincing proofs of the truth of that theory."

Using a crystal of aragonite, Lloyd succeeded in observing conical refraction. The experiment was difficult because the cone is narrow: the semi-angle A is small. If the slab has thickness l, the emerging cylinder, with radius

$$R_0 = Al, \tag{4.1}$$

is thin unless l is large. To see the cylinder clearly, R_0 must be larger than the width w of the incident beam. Lloyd used a beam narrowed by passage through small pinholes with radii $w \leqslant 200$ μm. As we will see, this interplay between R_0 and w is important. However, large l brings the additional difficulty of finding a

Table 1
Data for experiments on conical diffraction

Experiment	n_1, n_2, n_3	A (°)	l (mm)	w (μm)	ρ_0
Lloyd [1837] (aragonite)	1.5326, 1.6863, 1.6908	0.96	12	$\leqslant 200$	$\geqslant 1.0$
Potter [1841] (aragonite)	1.5326, 1.6863, 1.6908	0.96	12.7	12.7	16.7
Raman, Rajagopalan and Nedungadi [1941] (naphthalene)	1.525, 1.722, 1.945	6.9	2	0.5	500
Schell and Bloembergen [1978a] (aragonite)	1.530, 1.680, 1.695	1.0	9.5	21.8	7.8
Mikhailychenko [2005] (sulfur)	data not provided	3.5	30	17	56
Fève, Boulanger and Marnier [1994] (sphere of KTP = $KTiOPO_4$)	1.7636, 1.7733, 1.8636	0.92	2.56	53.0	1210
Berry, Jeffrey and Lunney [2006] (MDT = $KGd(WO_4)_2$	2.02, 2.06, 2.11	1.0	25	7.1	60

For the experiments of Lloyd and Raman, w is the pinhole radius; for the other experiments, w is the $1/e$ intensity half-width of the laser beam.

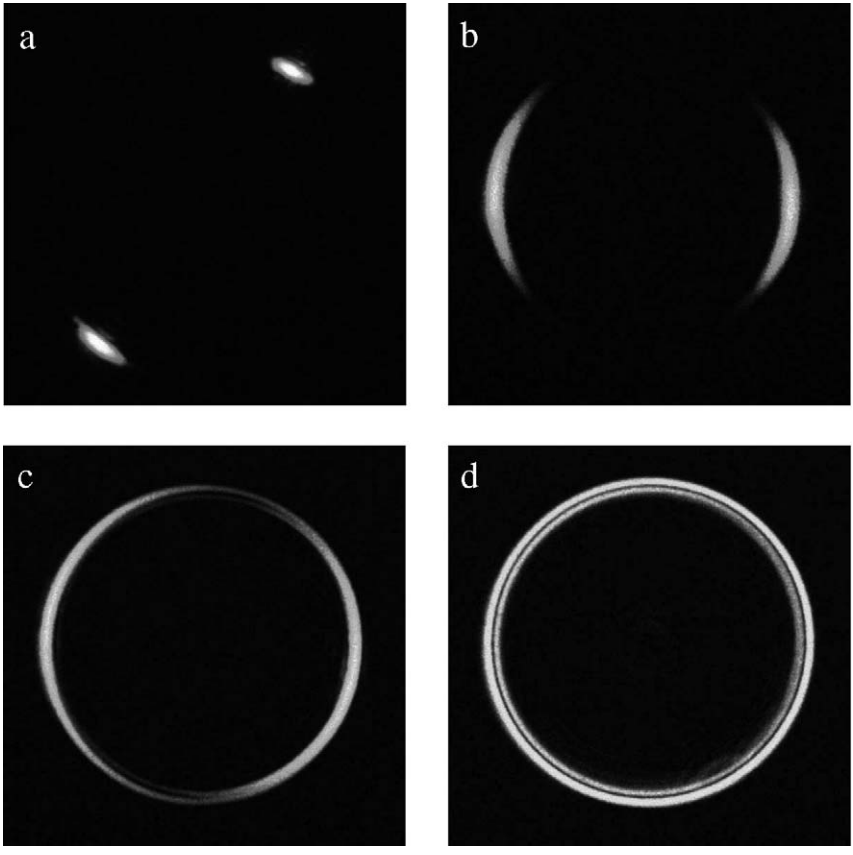

Fig. 5. The transition (a–d) from double to conical refraction as the incident beam direction approaches the optic axis. In (d) two rings are visible, separated by the Poggendorff dark ring studied in Section 5. This figure is taken from Berry, Jeffrey and Lunney [2006] (see also Table 1).

clean enough length of crystal; Lloyd describes how he explored several regions of his crystal before being able to detect the effect.

Nowadays it is simpler to use a laser beam with waist width w rather than a pinhole with radius w. Nevertheless, observation of the effect remains challenging. Table 1 summarises the conditions of the several experiments known to us; we will describe some of them later.

Figure 5 illustrates how double refraction transforms into conical refraction as the direction of the incident light beam approaches an optic axis. Of this transformation, Lloyd [1837] wrote: "This phenomenon was exceedingly striking. It looked like a small ring of gold viewed upon a dark ground; and the sudden and

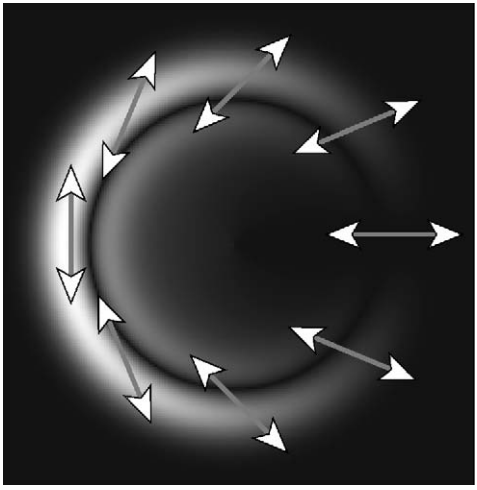

Fig. 6. Simulation of rings for incident beam linearly polarized horizontally, with polarization directions superimposed, showing the 'fermionic' half-turn of the polarization.

almost magical change of the appearance, from two luminous points to a perfect luminous ring, contributed not a little to enhance the interest."

Lloyd also observed a feature that Hamilton had predicted: the half-turn of polarization round the ring (fig. 6).

§ 5. Poggendorff's dark ring, Raman's bright spot

Hamilton was aware that his geometrical theory did not give a complete description of conical refraction: "I suspect the *exact* laws of it depend on things yet unknown" (Graves [1882]). And indeed, as fig. 5(d) shows, closer observation reveals internal structure in Hamilton's ring, that he did not predict and Lloyd did not detect: there is not one bright ring but two, separated by a dark ring. This was first reported in a brief but important paper by Poggendorff [1839] (fig. 1), who noted ". . .a bright ring that encompasses a coal-black sliver" ("einem hellen Ringe vereinigen, der ein kohlschwarzes Scheibchen einschliefst"). The existence of two bright rings, rather than one, was independently discovered soon afterwards by Potter [1841] (Table 1).

After more than 65 years, the origin of Poggendorff's dark ring was identified by Voigt [1905a] (fig. 1) (see also Born and Wolf [1999]), who pointed out that Hamilton's prediction involved the idealization of a perfectly collimated infinitely narrow beam. This is incompatible with the wave nature of light: a beam

of spatial width w must contain transverse wavevector components (i.e., k_x, k_y) extending over at least a range $1/w$ (more, if the light is incoherent); this is just the optical analogue of the uncertainty principle. Therefore the incident beam will explore not just the diabolical point itself but a neighbourhood of the optic axis in **k** space. In fact Hamilton knew about the off-axis waves: "it was in fact from considering them and passing to the limit that I first deduced my expectation of conical refraction". Lloyd too was aware of "the angle of divergence produced by diffraction in the minutest apertures".

Voigt's observation was that the strength of the light generated by the off-axis waves inside and outside the cylinder is proportional to the radius $\sqrt{k_x^2 + k_y^2}$ of the circumference of contributing rings on the wave cone. At the diabolical point this vanishes, so the intensity is zero on the geometrical cylinder itself. Thus, the Poggendorff dark ring is a manifestation of the area element in plane polar coordinates in **k** space.

The elementary quantitative theory of the Poggendorff ring is based on geometrical optics, incorporating the finite **k** width of the beam – which of course is a consequence of wave physics. Rigorous geometrical-optics treatments were given by Ludwig [1961] and Uhlmann [1982]; here, our aim is to obtain the simplest explicit formulae. To prepare for later analysis of experiments, we formulate the theory so as to describe the light beyond the crystal. Appropriately enough, we will use Hamilton's principle.

We begin with the optical path lengths from a point $\mathbf{r}_i$ on the entrance face $z = 0$ of the crystal to a point $\mathbf{r}$ beyond the crystal at a distance z from the entrance face, for the two waves with transverse wavevector components k_x, k_y:

$$\text{path length} = k_x(x - x_\mathrm{i}) + k_y(y - y_\mathrm{i}) + l\sqrt{k_0^2 n_{\mathbf{k}\pm}^2 - k_x^2 - k_y^2} + (z - l)\sqrt{k_0^2 - k_x^2 - k_y^2}. \tag{5.1}$$

The exit face of the crystal is $z = l$, but all our formulae are also valid for $z < l$, corresponding to observations, made with lenses outside the crystal, of the virtual field inside the crystal, as was appreciated long ago by Potter [1841], and later by Raman [1941] and Raman, Rajagopalan and Nedungadi [1941].

For the geometrical theory and all subsequent analysis, we will use the following dimensionless variables (fig. 7):

$$\begin{aligned} \boldsymbol{\rho} &= \{\xi, \eta\} = \rho\{\cos\phi, \sin\phi\} \equiv \frac{1}{w}\{x + R_0, y\}, \\ \boldsymbol{\kappa} &= \{\kappa_x, \kappa_y\} = \kappa\{\cos\phi_{\boldsymbol{\kappa}}, \sin\phi_{\boldsymbol{\kappa}}\} \equiv w\{k_x, k_y\}, \\ \rho_0 &\equiv \frac{R_0}{w}. \end{aligned} \tag{5.2}$$

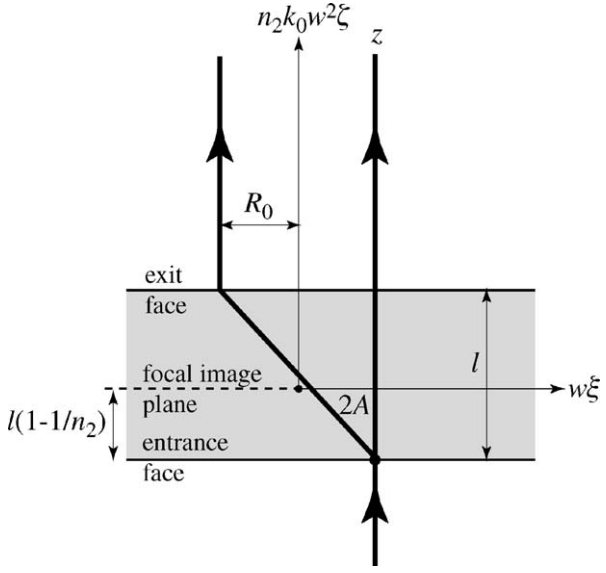

Fig. 7. Dimensionless coordinates for conical diffraction theory.

Here, transverse position $\boldsymbol{\rho}$ and transverse wavevectors $\boldsymbol{\kappa}$ are measured in terms of the beam width w, with $\boldsymbol{\rho}$ measured from the axis of the cylinder. Especially important is the parameter ρ_0, giving the radius of the cylinder in units of w; this single quantity characterises the field of rays – and also of waves, as we shall see – replacing the five quantities n_1, n_2, n_3, l, w. Well-developed rings correspond to $\rho_0 \gg 1$.

Near the diabolical point, κ is small, so we can write the sheets of the wave surface as

$$n_{\mathbf{k}\pm} = n_2\left(1 + \frac{A(-\kappa_x \pm \kappa)}{k_0 n_2 w}\right). \tag{5.3}$$

Now comes an important simplification, to be used in all subsequent analysis: because all angles are small (Table 1), we use the paraxial approximation (Appendix 1) to expand the square roots in eq. (5.1). This leads to

$$\text{path length} = k_0(n_2 l + z - l) + \Phi_\pm(\boldsymbol{\kappa}, \boldsymbol{\rho}, \boldsymbol{\rho}_i), \tag{5.4}$$

where

$$\Phi_\pm(\boldsymbol{\kappa}, \boldsymbol{\rho}, \boldsymbol{\rho}_\mathrm{i}) \equiv \boldsymbol{\kappa} \cdot (\boldsymbol{\rho} - \boldsymbol{\rho}_\mathrm{i}) \pm \kappa\rho_0 - \frac{1}{2}\kappa^2\zeta \tag{5.5}$$

and

$$\zeta \equiv \frac{l + n_2(z - l)}{n_2 k_0 w^2}. \tag{5.6}$$

Here ζ is a dimensionless propagation parameter, measuring distance from the 'focal image plane' $z = l(1 - 1/n_2)$ (fig. 7) where the sharpest image of the incident beam (pinhole or laser waist) would be formed if the crystal were isotropic (i.e., if A were zero). The importance of the focal image plane $\zeta = 0$ was first noted in observations by Potter [1841].

By Hamilton's principle, rays from $\{\boldsymbol{\rho}_\mathrm{i}, 0\}$ to $\{\boldsymbol{\rho}, z\}$ correspond to waves with wavenumber $\boldsymbol{\kappa}$ for which the optical distance is stationary. Thus

$$\nabla_{\boldsymbol{\kappa}} \Phi = \boldsymbol{\rho} - \boldsymbol{\rho}_\mathrm{i} \pm \rho_0 \mathbf{e}_{\boldsymbol{\kappa}} - \boldsymbol{\kappa}\zeta = 0, \tag{5.7}$$

that is

$$\boldsymbol{\rho} - \boldsymbol{\rho}_\mathrm{i} = (\kappa\zeta \mp \rho_0)\mathbf{e}_{\boldsymbol{\kappa}}. \tag{5.8}$$

Consider for the moment rays from $\boldsymbol{\rho}_\mathrm{i} = 0$. Squaring eq. (5.8) and using $\rho > 0$, $\kappa > 0$ leads to

$$\begin{aligned} &+\text{: two solutions: (a): } \boldsymbol{\kappa} = \frac{(\rho + \rho_0)}{\zeta}\mathbf{e}_{\boldsymbol{\rho}}, \\ &\qquad\qquad \text{(b): } \boldsymbol{\kappa} = \frac{(\rho_0 - \rho)}{\zeta}\mathbf{e}_{\boldsymbol{\rho}} \quad (\rho \leqslant \rho_0), \\ &-\text{: one solution: (c): } \boldsymbol{\kappa} = \frac{(\rho - \rho_0)}{\zeta}\mathbf{e}_{\boldsymbol{\rho}} \quad (\rho \geqslant \rho_0). \end{aligned} \tag{5.9}$$

For each ρ, there are two solutions: (a); and either (b) (if $\rho \leqslant \rho_0$) or (c) (if $\rho \geqslant \rho_0$). As fig. 8 illustrates, these correspond to minus the slopes of the surface

$$\frac{1}{2}\kappa^2\zeta \mp \kappa\rho_0. \tag{5.10}$$

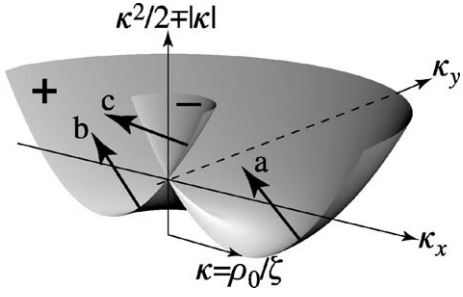

Fig. 8. The 'Hamiltonian' surface (5.10) whose normals generate the paraxial rays.

A ray bundle $\mathrm{d}\boldsymbol{\kappa}$ will reach $\mathrm{d}\boldsymbol{\rho}$ at ζ with intensity proportional to $|J|^{-1}$ where J is the Jacobian

$$J = \det \frac{\mathrm{d}\boldsymbol{\rho}}{\mathrm{d}\boldsymbol{\kappa}} = \det \frac{\partial(\xi, \eta)}{\partial(\kappa_x, \kappa_y)} = \zeta\left(\zeta \mp \frac{\rho_0}{\kappa}\right). \tag{5.11}$$

The ray equation (5.8) gives

$$|J|^{-1} = \frac{\kappa}{\zeta\rho} = \frac{|\rho \pm \rho_0|}{\zeta^2\rho}, \tag{5.12}$$

which for the minus sign vanishes linearly on the cylinder $\rho = \rho_0$, where, from (5.9), the contributing wavevector is the diabolical point $\kappa = 0$. Thus the Poggendoff dark ring is an 'anticaustic'.

This geometrical theory also explains an important observation made by Raman, Rajagopalan and Nedungadi [1941] (fig. 1), who emphasized that the ring pattern changes dramatically beyond the crystal; in our notation, the pattern depends strongly on the distance ζ from the focal image plane. Raman saw that as ζ increases, a bright spot develops at $\rho = 0$. This is associated with the factor $1/\rho$ in the inverse Jacobian (5.12), corresponding to a singularity on the cylinder axis $\rho = 0$ – a line caustic, resulting from the ring of normals where the surface (5.10) turns over at $\kappa = \rho_0/\zeta$ (fig. 8). At the turnover, the surface is locally toroidal, so the Raman spot is analogous to the optical glory (Nussenzveig [1992], van de Hulst [1981]) − another consequence of an axial caustic resulting from circular symmetry. Raman, Rajagopalan and Nedungadi [1941] pointed out that the turnover is related to the circle of contact in external conical refraction, so that the two effects discovered by Hamilton cannot be completely separated. The central spot had been observed earlier by Potter [1841], who however failed to understand its origin.

Since the factor $1/\rho$ in (5.12) applies to all z, why does the Raman spot appear only as ζ increases? The reason is that in the full geometrical-optics intensity I_{geom}, the inverse Jacobian must be modulated by the angular distribution of the incident beam. Let the incident transverse beam amplitude (assumed circular) have Fourier transform $a(\kappa)$. Important cases are a pinhole with radius w, and a Gaussian beam with intensity $1/e$ half-width w, for which [in the scaled variables (5.2)]

$$\begin{aligned} &\text{circular pinhole: } a_{\mathrm{p}}(\kappa) = \frac{J_1(\kappa)}{\kappa}, \\ &\text{Gaussian beam: } a_{\mathrm{G}}(\kappa) = \exp\left(-\frac{1}{2}\kappa^2\right). \end{aligned} \tag{5.13}$$

Incorporating the Jacobian and the ray equations gives

$$I_{\text{geom}}(\rho,\zeta)=\frac{1}{2\zeta^2\rho}\big[|\rho-\rho_0|\big|a\big(|\rho-\rho_0|/\zeta\big)\big|^2 + (\rho+\rho_0)\big|a\big((\rho+\rho_0)/\zeta\big)\big|^2\big]. \tag{5.14}$$

The first term represents the bright rings, separated by the Poggendorff dark ring; in this approximation, the rings are symmetric. The second term is weak except near $\rho=0$, where it combines with the first term to give the Raman central spot, with strength proportional to

$$\frac{1}{\rho\zeta^2}\big|a(\rho_0/\zeta)\big|^2, \tag{5.15}$$

which (for a Gaussian beam, for example) is exponentially small unless ζ approaches ρ_0, and decays slowly with ζ thereafter.

Although I_{geom} captures some essential features of conical refraction, it fails to describe others. Like all applications of geometrical optics, it neglects interference and polarization, and fails where there are geometrical singularities. Here the singularities are of two kinds: a zero at the anticaustic cylinder $\rho=\rho_0$, and focal divergences on the axial caustic $\rho=0$ and in the focal image plane $\zeta=0$.

Interference and polarization can be incorporated by adding the geometrical amplitudes (square roots of Jacobians) rather than intensities, with phases given by the values of $\Phi_\pm$ (from eq. (5.5)) at the contributing $\boldsymbol{\kappa}$ values. We will return to improvements of geometrical-optics theory in Section 7, and compare a more sophisticated version with exact wave theory (see fig. 12 later).

The singularity at $\zeta=0$ is associated with our choice of $\boldsymbol{\rho}_{\text{i}}=0$. Thus, although I_{geom} incorporates the effect of w on the angular spectrum of the incident beam, it neglects the more elementary lateral smoothing of the cylinder of conical refraction. One possible remedy is to average I_{geom} over points $\boldsymbol{\rho}_{\text{i}}$, that is, across the incident beam. In the focal image plane, where the unsmoothed I is singular, such averaging would obscure the Poggendorff dark ring. However, averaging over $\boldsymbol{\rho}_{\text{i}}$ is correct only for incoherent illumination, which does not correspond to Lloyd's and later experiments, where the light is spatially coherent. The correct treatment of the focal image plane, and of other features of the observed rings, requires a full wave theory.

§ 6. Belsky and Khapalyuk's exact paraxial theory of conical diffraction

Nearly 40 years after Raman, the need for a full wave treatment, based on an angular superposition of plane waves, was finally appreciated. Following (and

correcting) an early attempt by Lalor [1972], Schell and Bloembergen [1978a] supplied such a theory, but this was restricted to the exit face of the crystal (that is, it did not incorporate the ζ dependence of the ring pattern); moreover, it was unnecessarily complicated because it did not exploit the simplifying feature of paraxiality. The breakthrough was provided by Belsky and Khapalyuk [1978], who did make use of paraxiality and gave definitive general formulae, obtained after "quite lengthy calculations", which they omitted. We now give an elementary derivation of the same formulae.

The field $\mathbf{D} = \{D_x, D_y\}$ outside the crystal is a superposition of plane waves $\boldsymbol{\kappa}$, each of which is the result of a unitary 2×2 matrix operator $\mathbf{U}(\boldsymbol{\kappa})$ acting on the initial vector wave amplitude $\mathbf{a}(\boldsymbol{\kappa})$. Thus

$$\mathbf{D} = \frac{1}{2\pi} \iint \mathrm{d}\boldsymbol{\kappa} \exp\{\mathrm{i}\boldsymbol{\kappa} \cdot \boldsymbol{\rho}\}\mathbf{U}(\boldsymbol{\kappa})\mathbf{a}(\boldsymbol{\kappa}). \tag{6.1}$$

$\mathbf{U}(\boldsymbol{\kappa})$ is determined from two requirements: its eigenphases must be the $\boldsymbol{\rho}$-independent part of the phases $\Phi_\pm$ (5.5), involving the refractive indices $n_\pm(\boldsymbol{\kappa})$, and because the diabolical point at $\boldsymbol{\kappa} = 0$ is a degeneracy, its eigenvectors (the eigenpolarizations) must change sign as $\phi_{\boldsymbol{\kappa}}$ changes by 2π. These are satisfied by

$$\mathbf{U}(\boldsymbol{\kappa}) = \exp\{-\mathrm{i}\mathbf{F}(\boldsymbol{\kappa})\}, \tag{6.2}$$

where

$$\begin{aligned}\mathbf{F}(\boldsymbol{\kappa}) &= \frac{1}{2}\kappa^2\zeta \begin{pmatrix} 1 & 0 \\ 0 & 1 \end{pmatrix} + \rho_0\kappa \begin{pmatrix} \cos\phi_{\boldsymbol{\kappa}} & \sin\phi_{\boldsymbol{\kappa}} \\ \sin\phi_{\boldsymbol{\kappa}} & -\cos\phi_{\boldsymbol{\kappa}} \end{pmatrix} \\ &= \frac{1}{2}\kappa^2\zeta\mathbf{1} + \rho_0\kappa \cdot \mathbf{S},\end{aligned} \tag{6.3}$$

in which the compact form involves two of the Pauli spin matrices

$$\boldsymbol{\kappa} \cdot \mathbf{S} = \boldsymbol{\sigma}_3\kappa_x + \boldsymbol{\sigma}_1\kappa_y. \tag{6.4}$$

Evaluating the matrix exponential (6.2) gives the explicit form

$$\mathbf{U}(\boldsymbol{\kappa}) = \exp\left\{-\frac{1}{2}\mathrm{i}\kappa^2\zeta\right\}\left[\cos\rho_0\kappa\mathbf{1} - \mathrm{i}\frac{\sin\rho_0\kappa}{\kappa}\boldsymbol{\kappa} \cdot \mathbf{S}\right]. \tag{6.5}$$

We learned from A. Newell of a connection between the evolution associated with $\mathbf{U}(\boldsymbol{\kappa})$ and analytic functions. Although we do not make use of this connection, it is interesting, and we describe it in Appendix 2.

It is not hard to show that $\mathbf{U}(\boldsymbol{\kappa})$ possesses the required eigenstructure, namely

$$\mathbf{U}(\boldsymbol{\kappa})\mathbf{d}_\pm(\boldsymbol{\kappa}) = \lambda_\pm(\boldsymbol{\kappa})\mathbf{d}_\pm(\boldsymbol{\kappa}), \tag{6.6}$$

where

$$\lambda_{\pm}(\boldsymbol{\kappa}) = \exp\left\{\mathrm{i}\left(-\frac{1}{2}\kappa^2\zeta \pm \rho_0\kappa\right)\right\},$$

$$\mathbf{d}_{+}(\boldsymbol{\kappa}) = \begin{pmatrix} \cos\frac{1}{2}\phi_{\boldsymbol{\kappa}} \\ \sin\frac{1}{2}\phi_{\boldsymbol{\kappa}} \end{pmatrix}, \qquad \mathbf{d}_{-}(\boldsymbol{\kappa}) = \begin{pmatrix} \sin\frac{1}{2}\phi_{\boldsymbol{\kappa}} \\ -\cos\frac{1}{2}\phi_{\boldsymbol{\kappa}} \end{pmatrix}. \tag{6.7}$$

Without significant loss of generality, we can regard the incident beam as uniformly polarized and circularly symmetric, that is

$$\mathbf{a}(\boldsymbol{\kappa}) = a(\kappa)\begin{pmatrix} d_{0x} \\ d_{0y} \end{pmatrix} = a(\kappa)\mathbf{d}_0, \tag{6.8}$$

where $a(\kappa)$ is the Fourier amplitude introduced in the previous section [cf. eq. (5.13)], related to the transverse incident beam profile $D_0(\rho)$ by

$$\mathbf{D}_0 = \mathbf{d}_0 D_0(\rho) = \mathbf{d}_0 \int_0^\infty \mathrm{d}\kappa\, \kappa J_0(\kappa\rho) a(\kappa). \tag{6.9}$$

Combining eqs. (6.1), (6.5) and (6.9), we obtain, after elementary integrations, and recalling $\boldsymbol{\rho} = \rho\{\cos\phi, \sin\phi\}$,

$$\mathbf{D} = \begin{pmatrix} B_0 + B_1\cos\phi & B_1\sin\phi \\ B_1\sin\phi & B_0 - B_1\cos\phi \end{pmatrix}\mathbf{d}_0, \tag{6.10}$$

where

$$B_0(\rho, \zeta; \rho_0) = \int_0^\infty \mathrm{d}\kappa\, \kappa a(\kappa) \exp\left\{-\frac{1}{2}\mathrm{i}\zeta\kappa^2\right\} J_0(\kappa\rho)\cos(\kappa\rho_0),$$

$$B_1(\rho, \zeta; \rho_0) = \int_0^\infty \mathrm{d}\kappa\, \kappa a(\kappa) \exp\left\{-\frac{1}{2}\mathrm{i}\zeta\kappa^2\right\} J_1(\kappa\rho)\sin(\kappa\rho_0). \tag{6.11}$$

These are the fundamental integrals of the Belsky–Khapalyuk theory.

For unpolarized or circularly polarized incident light, eq. (6.10) gives the intensity as

$$I = \mathbf{D}^* \cdot \mathbf{D} = |B_0|^2 + |B_1|^2. \tag{6.12}$$

A useful alternative form for $\mathbf{D}$, in terms of the eigenvectors $\mathbf{d}_{\pm}$ evaluated at the direction ϕ of $\boldsymbol{\rho}$, and involving

$$A_+ \equiv B_0 + B_1, \qquad A_- \equiv B_0 - B_1, \tag{6.13}$$

is

$$\mathbf{D} = A_+\left(d_{0x}\cos\frac{1}{2}\phi + d_{0y}\sin\frac{1}{2}\phi\right)\mathbf{d}_+(\rho) + A_-\left(d_{0x}\sin\frac{1}{2}\phi - d_{0y}\cos\frac{1}{2}\phi\right)\mathbf{d}_-(\rho). \tag{6.14}$$

$\mathbf{D}$ is a single-valued function of $\boldsymbol{\rho}$, although $\mathbf{d}_\pm(\boldsymbol{\rho})$ change sign around the origin. The corresponding intensity,

$$I = |A_+|^2\left|d_{0x}\cos\frac{1}{2}\phi + d_{0y}\sin\frac{1}{2}\phi\right|^2 + |A_-|^2\left|d_{0x}\sin\frac{1}{2}\phi - d_{0y}\cos\frac{1}{2}\phi\right|^2, \tag{6.15}$$

contains no oscillations resulting from interference between A_+ and A_-, because $\mathbf{d}_+$ and $\mathbf{d}_-$ are orthogonally polarized. But, as we will see in the next section, the exact rings do possess oscillations, from A_+ and A_- individually.

Associated with the polarization structure of the beam (6.14) (see also fig. 6) is an interesting property of the angular momentum (Berry, Jeffrey and Mansuripur [2005]): for well-developed rings (large ρ_0), the initial angular momentum, which is pure spin, is transformed by the crystal into pure orbital, and reduced in magnitude, the difference being imparted to the crystal.

§ 7. Consequences of conical diffraction theory

We begin our explanation of the rich implications of the paraxial wave theory by obtaining an explicit expression for the improved geometrical-optics theory anticipated in Section 5. The derivation proceeds by replacing the Bessel functions in eq. (6.11) by their asymptotic forms, and then evaluating the integrals by their stationary-phase approximations. The stationary values of κ specify the rays (5.9), and the result, for the quantities $A_\pm$, is:

$$A_{+\mathrm{geom}} = \frac{\sqrt{|\rho_0-\rho|}}{\zeta\sqrt{\rho}}a\left(\frac{|\rho_0-\rho|}{\zeta}\right)\exp\left\{\mathrm{i}\frac{(\rho_0-\rho)^2}{2\zeta}\right\}\times\begin{pmatrix}1 \text{ if } \rho<\rho_0\\ -\mathrm{i} \text{ if } \rho>\rho_0\end{pmatrix},$$
$$A_{-\mathrm{geom}} = -\mathrm{i}\frac{\sqrt{\rho_0+\rho}}{\zeta\sqrt{\rho}}a\left(\frac{\rho_0+\rho}{\zeta}\right)\exp\left\{\mathrm{i}\frac{(\rho_0+\rho)^2}{2\zeta}\right\}. \tag{7.1}$$

For an incident beam linearly polarized in direction γ, that is

$$\mathbf{d}_0 = \begin{pmatrix}\cos\gamma\\ \sin\gamma\end{pmatrix}, \tag{7.2}$$

the resulting electric field (6.14) is

$$\mathbf{D} = A_{+\mathrm{geom}} \cos\left(\frac{1}{2}\phi - \gamma\right)\mathbf{d}_+(\phi) + A_{-\mathrm{geom}} \sin\left(\frac{1}{2}\phi - \gamma\right)\mathbf{d}_-(\phi), \quad (7.3)$$

and the intensity is

$$I_{\mathrm{geom1}} = \mathbf{D}^* \cdot \mathbf{D} = \left[|A_{+\mathrm{geom}}|^2 \cos^2\left(\frac{1}{2}\phi - \gamma\right) + |A_{-\mathrm{geom}}|^2 \sin^2\left(\frac{1}{2}\phi - \gamma\right)\right]. \quad (7.4)$$

The elementary geometrical-optics intensity I_{geom} (5.14) is recovered for unpolarized light by averaging over γ, or by superposing intensities for any two orthogonal incident polarizations. Without such averaging, the first term in I_{geom1} gives the lune-shaped ring structure observed by Lloyd (fig. 6) with linearly polarized light, and both terms combine to give the unpolarized geometrical central spot.

Next, we examine the detailed structure of the Poggendorff rings, starting with the focal image plane $\zeta = 0$ where the rings are most sharply focused. Figure 9

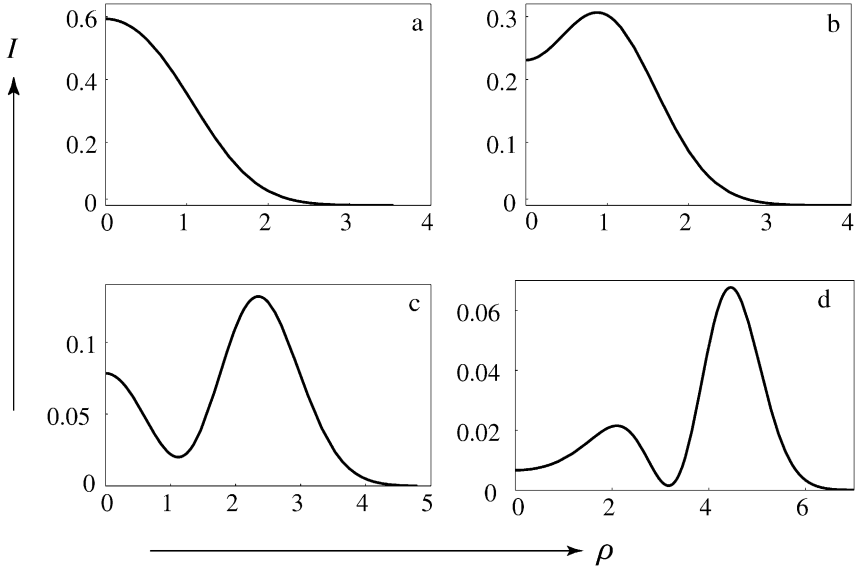

Fig. 9. Emergence of double ring structure in the focal image plane $\zeta = 0$ as ρ_0 increases, computed from eq. (6.10) for an unpolarized Gaussian incident beam. (a) $\rho_0 = 0.5$; (b) $\rho_0 = 0.8$; (c) $\rho_0 = 2$; (d) $\rho_0 = 4$.

shows how the double ring emerges as ρ_0 increases. Significant events, corresponding to sign changes in the curvature of I at $\rho = 0$, are: the birth of the first ring when $\rho_0 = 0.627$; the birth of a central maximum when $\rho_0 = 1.513$; and the birth of the second bright ring when $\rho_0 = 2.669$.

As ρ_0 increases further, the rings become localized near $\rho = \rho_0$, but their shape is independent of ρ_0 and depends only on the form of the incident beam. To obtain a formula for this invariant shape, we cannot use geometrical optics for the large-ρ_0 asymptotics. The reason is that although eq. (7.1) is a good approximation to A_-, it fails for the function A_+ that determines the rings, because the ray contribution comes from the neighbourhood of the end-point $\kappa = 0$ of the integrals. So, although the Bessel functions can still be replaced by their asymptotic forms, the stationary-phase approximation is invalid. Near the rings, with

$$\Delta\rho \equiv \rho - \rho_0, \tag{7.5}$$

Bessel asymptotics gives A_+ as

$$A_{+\text{rings}} = \frac{1}{\sqrt{\rho}} f(\Delta\rho, \zeta), \tag{7.6}$$

where

$$f(\Delta\rho, \zeta) = \sqrt{\frac{2}{\pi}} \int_0^\infty \mathrm{d}\kappa \, \sqrt{\kappa} a(\kappa) \cos\left\{\kappa\Delta\rho - \frac{1}{4}\pi\right\} \exp\left\{-\frac{1}{2}\mathrm{i}\kappa^2\zeta\right\}. \tag{7.7}$$

In the focal image plane $\zeta = 0$, f can be evaluated analytically for a pinhole incident beam, in terms of elliptic integrals E and K. With the conventions in Mathematica (Wolfram [1996]),

$$f_{0\mathrm{p}}(\Delta\rho) \equiv f(\Delta\rho, 0)$$
$$= \begin{cases} \dfrac{2\sqrt{2}}{\pi}\left[\sqrt{1-\Delta\rho}\,E\left(\dfrac{2}{1-\Delta\rho}\right) + \dfrac{\Delta\rho}{\sqrt{1-\Delta\rho}}K\left(\dfrac{2}{1-\Delta\rho}\right)\right] \\ \quad (\Delta\rho < -1), \\ \dfrac{2}{\pi}\left[-K\left(\dfrac{1}{2}(1-\Delta\rho)\right) + 2E\left(\dfrac{1}{2}(1-\Delta\rho)\right)\right] \\ \quad (|\Delta\rho| < 1), \\ 0 \quad (\Delta\rho > 1). \end{cases} \tag{7.8}$$

Figure 10(a) shows the corresponding intensity. To our knowledge, this unusual focused image has not been seen in any experiment.

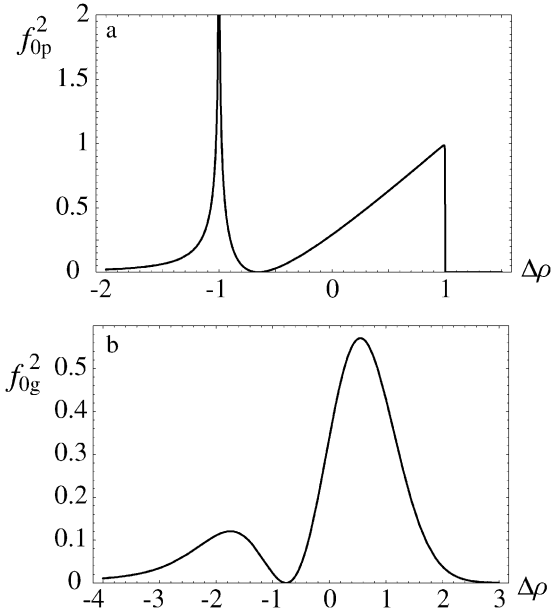

Fig. 10. Intensity functions $f_0^2(\Delta\rho)$ of rings in the focal image plane, for (a) a circular pinhole (7.8), and (b) a Gaussian beam (7.9).

For a Gaussian beam, the focal image can be expressed in terms of Bessel functions:

$$f_{0g}(\Delta\rho) \equiv f(\Delta\rho, 0) = \frac{|\Delta\rho|^{3/2}\exp\left(-\frac{1}{4}\Delta\rho^2\right)}{2\sqrt{2\pi}}\left[K_{\frac{3}{4}}\left(\frac{1}{4}\Delta\rho^2\right) + \operatorname{sgn}\Delta\rho\, K_{\frac{1}{4}}\left(\frac{1}{4}\Delta\rho^2\right) + \pi\sqrt{2}\Theta(-\Delta\rho)\left(I_{\frac{3}{4}}\left(\frac{1}{4}\Delta\rho^2\right) - I_{\frac{1}{4}}\left(\frac{1}{4}\Delta\rho^2\right)\right)\right]. \tag{7.9}$$

Figure 10(b) shows the corresponding intensity, and fig. 11 shows how the approximation f_{0g} gets better as ρ_0 increases. The focal image functions f_{0p} and f_{0g} have been discussed in detail by Belsky and Stepanov [1999], Berry [2004b] and Warnick and Arnold [1997]; of several equivalent representations, eqs. (7.8) and (7.9) are the most convenient.

Away from the focal image plane, that is as ζ increases from zero, secondary rings develop, in the form of oscillations within the inner bright ring [the solid curves in fig. 12(b–e)]; these were discovered in numerical computations by Warnick and Arnold [1997]. Using asymptotics based on eq. (7.7), the secondary

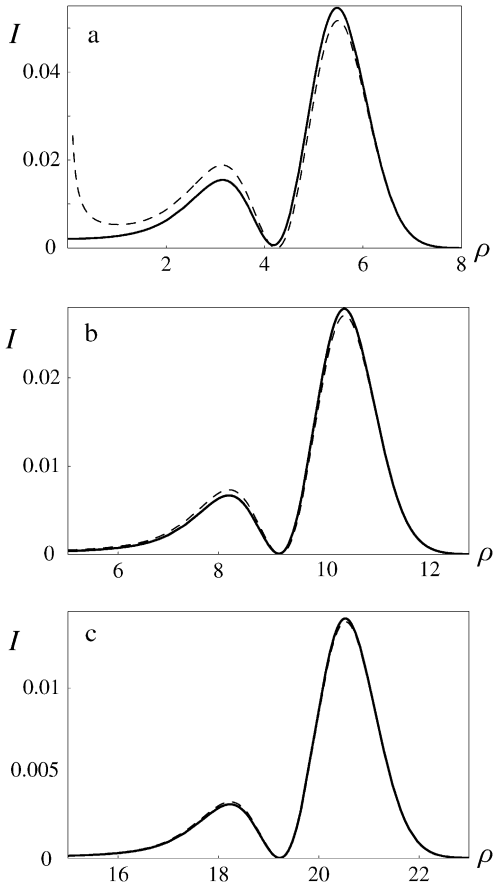

Fig. 11. Ring intensity in the focal image plane for a Gaussian incident beam, calculated exactly (solid curves), and in the local approximation (7.6) and (7.9) (dashed curves), for (a) $\rho_0 = 5$; (b) $\rho_0 = 10$; (c) $\rho_0 = 20$. [The divergences at $\rho = 0$ for the approximate rings come from the factor $1/\sqrt{\rho}$ in eq. (7.6).]

rings can be interpreted as interference between a geometrical ray and a wave scattered from the diabolical point in **k** space (Berry [2004b]); the associated mathematics led to a surprising general observation in the asymptotics of competing exponentials (Berry [2004a]).

All the features so far discussed are displayed in the simulated image and cutaway in fig. 13, which can be regarded as a summary of the main results of conical diffraction theory. The parameters ($\rho_0 = 20$, $\zeta = 8$) are chosen to display the two bright rings, the Poggendorff dark ring, the nascent Raman spot (whose intensity will increase for larger ζ), and the secondary rings.

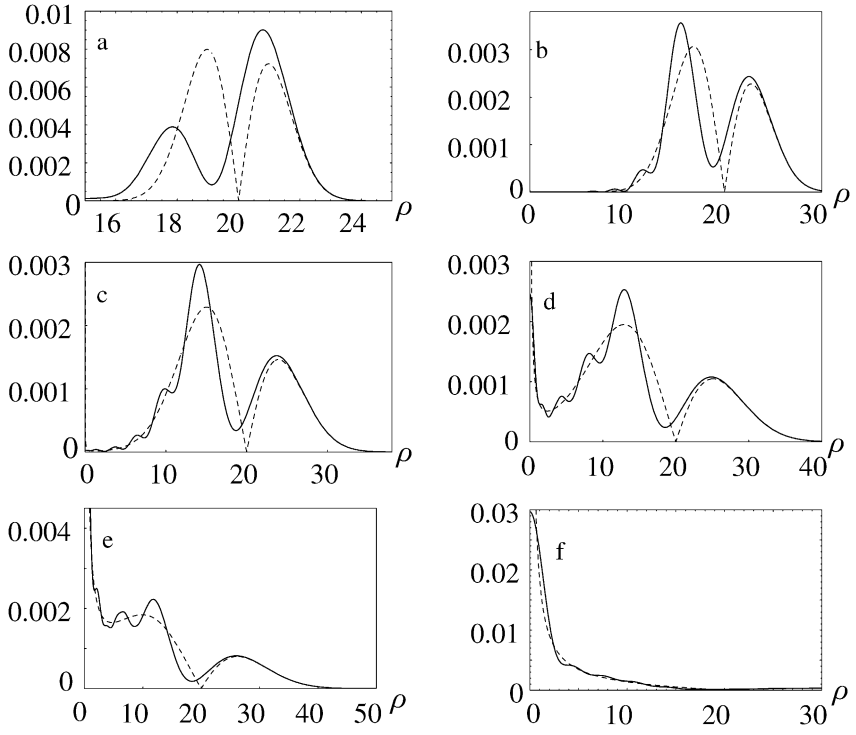

Fig. 12. Intensity for a Gaussian incident beam for $\rho_0 = 20$ and (a) $\zeta = 1$; (b) $\zeta = 4$; (c) $\zeta = 6$; (d) $\zeta = 8$; (e) $\zeta = 10$; (f) $\zeta = 20$. Solid curves: exact theory; dashed curves: refined geometrical-optics theory (7.13).

As ζ increases further, the inner rings approach the Raman spot [solid curves in fig. 12(e,f)], and are then described by Bessel functions (Berry [2004b]):

$$B_0(\rho,\zeta;\rho_0) \approx \rho_0\sqrt{\frac{\pi}{2\zeta^3}}\exp\left\{\mathrm{i}\left(\frac{\rho_0^2}{2\zeta}-\frac{1}{4}\pi\right)a\left(\frac{\rho_0}{\zeta}\right)J_0\left(\frac{\rho\rho_0}{\zeta}\right)\right\},$$

$$B_1(\rho,\zeta;\rho_0) \approx \rho_0\sqrt{\frac{\pi}{2\zeta^3}}\exp\left\{\mathrm{i}\left(\frac{\rho_0^2}{2\zeta}-\frac{3}{4}\pi\right)a\left(\frac{\rho_0}{\zeta}\right)J_1\left(\frac{\rho\rho_0}{\zeta}\right)\right\},$$

$$(\rho \ll \rho_0,\ \zeta \gg 1). \tag{7.10}$$

Figure 14 illustrates how well the approximation $J_0^2 + J_1^2$ approximates the true intensity. The weak oscillations (shoulders at zeros of $J_1(\rho\rho_0/\zeta)$) are the result of interference involving the next large-ρ_0 correction term to the geometrical-optics approximation (7.1).

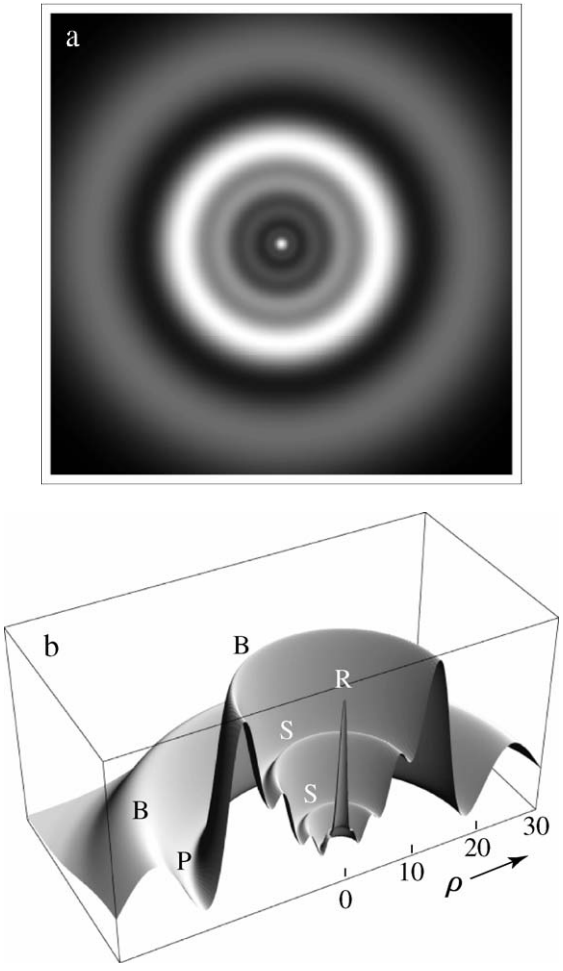

Fig. 13. (a) Density plot and (b) cutaway 3D plot, of conical diffraction intensity for $\rho_0 = 20$, $\zeta = 8$, showing bright rings B, Poggenforff dark ring P, Raman spot R and secondary rings S.

In the important special case of a Gaussian incident beam, the conical diffraction integrals (6.11) for general ζ can be obtained by complex continuation from the focal image plane $\zeta = 0$. This useful simplification is a variant of the complex-source trick of Deschamps [1971]. It is based on the observation

$$\exp\left\{-\frac{1}{2}\kappa^2\right\}\exp\left\{-\frac{1}{2}\mathrm{i}\kappa^2\zeta\right\} = \exp\left\{-\frac{1}{2}\kappa^2(1+\mathrm{i}\zeta)\right\}, \tag{7.11}$$

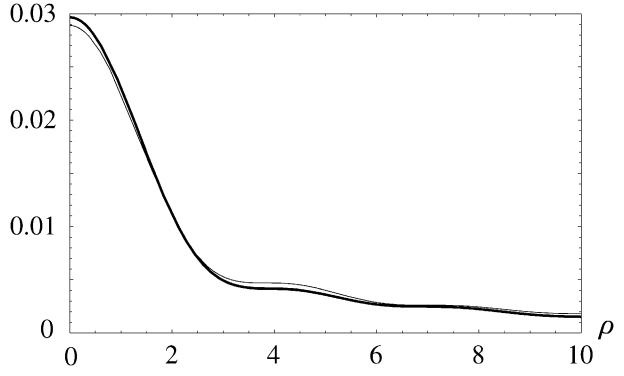

Fig. 14. Weak oscillations decorating the Raman spot for a Gaussian incident beam; thick curve: exact intensity; thin curve: Bessel approximation (7.10), for $\rho_0 = 20$, $\zeta = 20$.

and leads to

$$B_{0,1}(\rho, \zeta; \rho_0) = \frac{1}{1 + \mathrm{i}\zeta} B_{0,1}\left(\frac{\rho}{\sqrt{1 + \mathrm{i}\zeta}}, 0, \frac{\rho_0}{\sqrt{1 + \mathrm{i}\zeta}}\right). \tag{7.12}$$

In geometrical optics, the same trick leads to a further refinement, incorporating $a(\kappa)$ into the stationary-phase approximation (so that the rays are complex):

$$\begin{aligned} A_{+\mathrm{geom1}} &= \frac{\sqrt{|\rho_0 - \rho|}}{(\zeta - \mathrm{i})\sqrt{\rho}} \exp\left\{\mathrm{i}\zeta \frac{(\rho_0 - \rho)^2}{2(\zeta^2 + 1)}\right\} \\ &\quad \times \exp\left\{-\frac{(\rho_0 - \rho)^2}{2(\zeta^2 + 1)}\right\} \times \begin{pmatrix} 1 \text{ if } \rho < \rho_0 \\ -\mathrm{i} \text{ if } \rho > \rho_0 \end{pmatrix}, \\ A_{-\mathrm{geom1}} &= -\mathrm{i}\frac{\sqrt{\rho_0 + \rho}}{(\zeta - \mathrm{i})\sqrt{\rho}} \exp\left\{\mathrm{i}\zeta \frac{(\rho_0 + \rho)^2}{2(\zeta^2 + 1)}\right\} \exp\left\{-\frac{(\rho_0 + \rho)^2}{2(\zeta^2 + 1)}\right\}. \end{aligned} \tag{7.13}$$

Figure 12 shows how accurately this reproduces the oscillation-averaged rings and the Raman spot when ζ is not small. Near the focal plane, however, the geometrical approximation is only rough, even though the refinement eliminates the singularity at $\zeta = 0$.

§ 8. Experiments

Experimental studies of conical refraction are few, probably because of the difficulty of finding, or growing, crystals of sufficient quality and thickness. Table 1

lists the investigations known to us. We have already mentioned the pioneering observations of Lloyd, Poggendorff, Potter and Raman.

Lloyd [1837] stated that he used several pinholes, but gave only the size of the largest (which he used as a way of measuring A), so we do not know the values of w, and hence ρ_0, corresponding to his rings. Poggendorff [1839] gave no details of his experiment, except that it was performed with aragonite. Potter [1841] gave a detailed description of his experiments with aragonite, but misinterpreted his observation of the double ring as evidence against the diabolical connection of the sheets of the wave surface, leading to polemical criticisms of Hamilton and Lloyd. Raman, Rajagopalan and Nedungadi [1941] chose naphthalene, whose crystals have a large cone angle A and which they could grow in sufficient thickness. They emphasize that they did not see the Poggendorff dark ring in their most sharply focused images; but in the focal image plane the two bright rings are very narrow (comparable with $w \approx 0.5$ μm), so they might not have resolved them.

Schell and Bloembergen [1978a] compared measured ring profiles with numerically integrated wave theory and with the stationary-phase (geometrical optics) approximation, in a plane corresponding to the exit face of their aragonite crystal. From the data in Table 1, it follows that this corresponds to $\zeta \approx 1.3$, a regime in which there is no central spot and no secondary rings, and, as they report, geometrical optics is a reasonable approximation.

Perkal'skis and Mikhailychenko [1979] and Mikhailychenko [2005] report large-scale demonstrations of internal and external conical refraction with rhombic sulfur.

In an ingenious investigation, Fève, Boulanger and Marnier [1994] used KTP in the form of a ball rather than a slab. The theory of Section 6 applies, provided the parameters are interpreted as follows:

$$\rho_0 \to \rho_{\text{ball}} = \rho_0\left(1 - 2(n_2 - 1)\frac{d}{l}\right),$$
$$\zeta \to \zeta_{\text{ball}} = \frac{l + d(2 - n_2)}{n_2 k w^2}, \tag{8.1}$$

where l is the diameter of the ball and d is the distance between the exit face of the ball and the observation plane. In this case, a cone emerges from the ball, giving rings whose radius $w\rho_{\text{ball}}$ depends on d; the radius vanishes at a point, close to the ball, where the generators of the cone (that is, the rays) cross. They obtain good agreement between the measured ring profile and the geometrical-optics intensity, which is a good approximation in their regime of enormous effective ρ_0 and relatively modest ζ (Table 1).

The many wave-optical and geometrical-optical phenomena predicted by the detailed theory of conical diffraction have recently been observed by Berry, Jef-

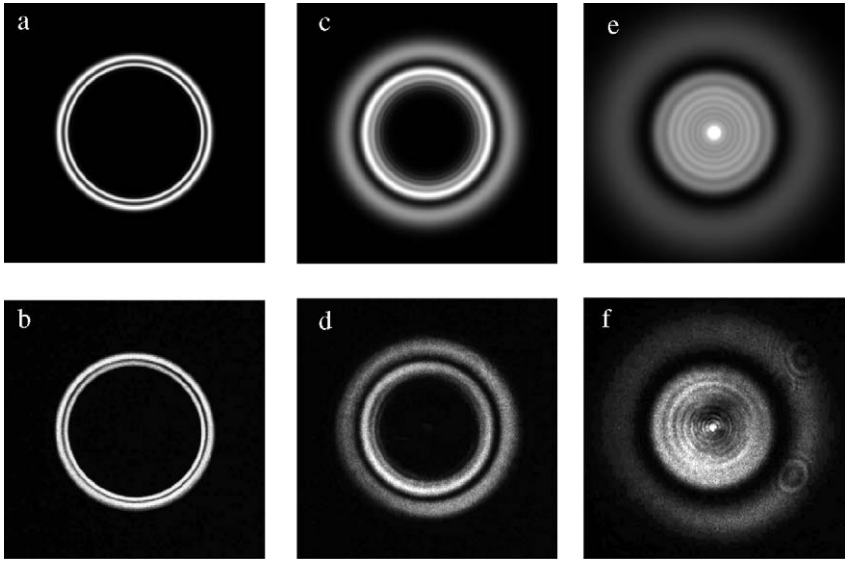

Fig. 15. Theoretical and experimental images for a monoclinic double tungstate crystal illuminated by a Gaussian beam (Berry, Jeffrey and Lunney [2006]), for $\rho_0 = 60$. (a,b) $\zeta = 3$; (c,d) $\zeta = 12$; (e,f) $\zeta = 30$; (a,c,e) theory; (b,d,f) experiment.

frey and Lunney [2006] in a crystal of the monoclinic double tungstate material $KGd(WO_4)_2$, obtained from Vision Crystal Technology (VCT [2006]). The agreement, illustrated in figs. 15 and 16, is quantitative as well as qualitative. Their measurements confirm predictions for the ζ-dependence of the radii and separation of the main rings, and of the sizes of the interference fringes: the secondary rings decorating the inner bright ring, and the rings decorating the Raman spot.

§ 9. Concluding remarks

Although conical diffraction exemplifies a fundamental feature of crystal optics, namely the diabolical point, it can also be regarded as a curiosity, because the effect seems to occur nowhere in the natural universe, and no practical application seems to have been found. To forestall confusion, we should immediately qualify these assertions.

It is Hamilton's idealized geometry (collimated beam, parallel-sided crystal slab, etc.) that does not occur in nature. In generic situations, for example an anisotropic medium that is also inhomogeneous, it is likely for a ray to encounter a

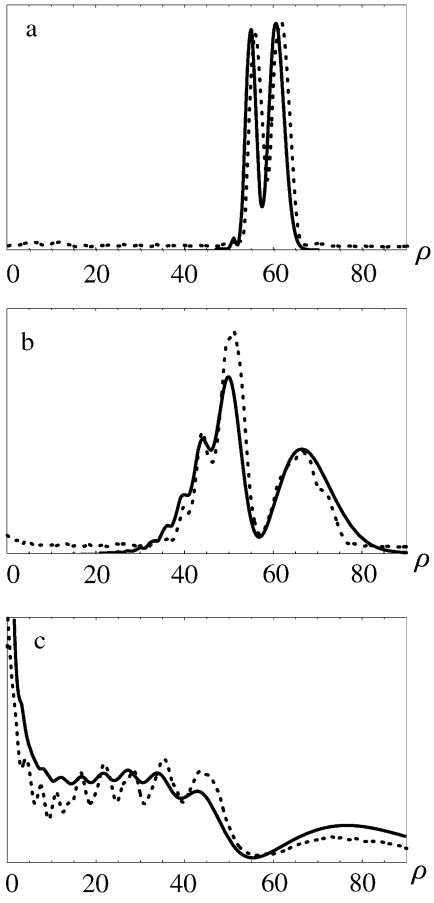

Fig. 16. As fig. 15, with (a) $\zeta = 3$; (b) $\zeta = 12$; (c) $\zeta = 30$. Solid curves: theory; dashed curves: angular averages of experimental images. (After Berry, Jeffrey and Lunney [2006].)

point where its direction is locally diabolical, corresponding to a local refractive-index degeneracy (Naida [1979]); or, in quantum mechanics, a coupled system with fast and slow components (e.g., a molecule) can encounter a degeneracy of the adiabatically evolving fast sub-system. In understanding such generic situations, the analysis of the idealized case will surely play a major part.

On the practical side, it is possible that the bright cylinder of conical refraction can be applied to trap and manipulate small particles; this is being explored, but the outcome is not yet clear. And a related phenomenon associated with the diabolical point, namely the conoscopic interference figures seen under polarized

illumination of very thin crystal plates, is a well-established identification technique in mineralogy (Liebisch [1896]).

As we have tried to explain, our understanding of the effect predicted by Hamilton is essentially complete. We end by describing several generalizations that are less well understood.

Although the theory of Section 6 applies to any paraxial incident beam, detailed explorations have been restricted to pinhole and Gaussian beams. A start has been made by King, Hogervorst, Kazak, Khilo and Ryzhevich [2001] and Stepanov [2002] in the exploration of other types of beam, for example Laguerre–Gauss and Bessel beams.

A further extension is to materials that are chiral (optically active) as well as biaxially birefringent. This alters the mathematical framework, because chirality destroys the diabolical point by separating the two sheets of the wave surface, reflecting the change of the dielectric matrix from real symmetric to complex Hermitian. There have been several studies incorporating chirality (Belsky and Stepanov [2002], Schell and Bloembergen [1978b], Voigt [1905b]), leading to the recent identification of the central new feature: the bright cylinder of conical refraction is replaced by a 'spun cusp' caustic (Berry and Jeffrey [2006a]). So far this has not been seen in any experiment.

The introduction of anisotropic absorption (dichroism) brings a more radical change: each diabolical point splits into two branch-points, reflecting the fact that the dielectric matrix is now non-Hermitian (Berry [2004c], Berry and Dennis [2003]). The dramatic effects of absorption on the pattern of emerging light have been recently described by Berry and Jeffrey [2006b]. The combined effects of dichroism and chirality have been described by Jeffrey [2007].

The final generalization incorporates nonlinearity. Early results were reported by Schell and Bloembergen [1977] and Shih and Bloembergen [1969], and the subject has been revisited by Indik and Newell [2006].

Acknowledgements

Our research is supported by the Royal Society. We thank Professor Alan Newell for permission to reproduce the argument in Appendix 2.

Appendix 1: Paraxiality

The paraxial approximation requires small angles, equivalent to replacing $\cos\theta$ by $1-\theta^2/2$, that is, to assuming $\theta^4/24 \ll 1$ for all wave deflection angles θ. In

conical refraction, deflections are determined by the half-angle of the ray cone, which from eq. (3.7) is

$$A = \frac{1}{2}\arctan\bigl(n_2^2\sqrt{\alpha\beta}\bigr). \tag{A.1}$$

This is indeed small in practice, because of the near-equality of the three refractive indices. For the Lloyd [1837] experiment on aragonite, the Berry, Jeffrey and Lunney [2006] experiment on MDT, and the Raman, Rajagopalan and Nedungadi [1941] experiment on naphthalene (whose cone angle is the largest yet reported), the data in Table 1 give

$$\begin{aligned}
&\frac{1}{24}A_{\text{Lloyd}}^4 = 3.3\times10^{-9},\\
&\frac{1}{24}A_{\text{Berry}}^4 = 9.1\times10^{-9},\\
&\frac{1}{24}A_{\text{Raman}}^4 = 8.5\times10^{-6}.
\end{aligned} \tag{A.2}$$

As is often emphasized, internal and external conical refraction are associated with different aspects of the geometry of the wave surface. But in the paraxial regime the difference between the cone angles (A and A_{ext} respectively) disappears. To explore this, we first note that (Born and Wolf [1999])

$$A_{\text{ext}} = \frac{1}{2}\arctan\bigl(n_1n_3\sqrt{\alpha\beta}\bigr). \tag{A.3}$$

In terms of the refractive-index differences

$$\mu_1 \equiv \frac{n_2-n_1}{n_2}, \qquad \mu_3 \equiv \frac{n_3-n_2}{n_2}, \tag{A.4}$$

we have, to lowest order,

$$A \approx A_{\text{ext}} \approx \sqrt{\mu_1\mu_3}, \tag{A.5}$$

which is proportional to the refractive-index differences. The difference between the angles is

$$A - A_{\text{ext}} \approx \sqrt{\mu_1\mu_3}\biggl[\mu_1-\mu_3+\frac{1}{4}\bigl(3\mu_1^2-2\mu_1\mu_3+3\mu_3^2\bigr)\biggr], \tag{A.6}$$

which is proportional to the square of the index differences, except when the two differences are equal, when it is proportional to the cube. For the aragonite, MDT and naphthalene experiments,

$$\begin{aligned}
&A_{\text{Lloyd}} - A_{\text{ext,Lloyd}} = 8.9\times10^{-2}A_{\text{Lloyd}},\\
&A_{\text{Berry}} - A_{\text{ext,Berry}} = -4.4\times10^{-3}A_{\text{Berry}},\\
&A_{\text{Raman}} - A_{\text{ext,Raman}} = -2.7\times10^{-4}A_{\text{Raman}}.
\end{aligned} \tag{A.7}$$

Appendix 2: Conical refraction and analyticity

We seek the paraxial differential equation for the evolution of the wave inside the crystal. Within the framework of Section 6, the wave can be described by setting $z = l$ and regarding $\zeta = l/k_0 w^2$ as a variable, enabling the evolution operator (6.2) and (6.3) to be written as

$$\mathbf{U}(\boldsymbol{\kappa}) = \exp\left\{-\mathrm{i}\zeta\left(\frac{1}{2}\kappa^2\mathbf{1} + \Gamma\boldsymbol{\kappa}\cdot\mathbf{S}\right)\right\}, \tag{B.1}$$

where

$$\Gamma \equiv Ak_0 w. \tag{B.2}$$

Writing $\boldsymbol{\kappa}$ as the differential operator

$$\boldsymbol{\kappa} = -\mathrm{i}\nabla = -\mathrm{i}\{\partial_\xi, \partial_\eta\}, \tag{B.3}$$

and differentiating eq. (B.1) with respect to ζ leads to

$$\mathrm{i}\partial_\zeta \begin{pmatrix} D_\xi \\ D_\eta \end{pmatrix} = \left[-\frac{1}{2}\nabla^2 \begin{pmatrix} 1 & 0 \\ 0 & 1 \end{pmatrix} - \mathrm{i}\Gamma \begin{pmatrix} \partial_\xi & \partial_\eta \\ \partial_\eta & -\partial_\xi \end{pmatrix}\right] \begin{pmatrix} D_\xi \\ D_\eta \end{pmatrix}. \tag{B.4}$$

The differential operator connects the components of $\mathbf{D}$ in the same way as the Cauchy–Riemann conditions for analytic functions. The relation is clearer when $\mathbf{D}$ is expressed in a basis of circular polarizations and ξ and η are replaced by complex variables, as follows

$$\begin{aligned} &D_+ \equiv \frac{1}{\sqrt{2}}(D_\xi - \mathrm{i}D_\eta), \qquad D_- \equiv \frac{1}{\sqrt{2}}(D_\xi + \mathrm{i}D_\eta), \\ &w_+ \equiv \xi + \mathrm{i}\eta, \qquad w_- \equiv \xi - \mathrm{i}\eta. \end{aligned} \tag{B.5}$$

Then eq. (B.4) becomes

$$\mathrm{i}\partial_\zeta \begin{pmatrix} D_+ \\ D_- \end{pmatrix} = -2\left[\partial_{w_+}\partial_{w_-} \begin{pmatrix} 1 & 0 \\ 0 & 1 \end{pmatrix} + \mathrm{i}\Gamma \begin{pmatrix} 0 & \partial_{w_+} \\ \partial_{w_-} & 0 \end{pmatrix}\right] \begin{pmatrix} D_+ \\ D_- \end{pmatrix}. \tag{B.6}$$

Thus D_+ and D_- propagate unchanged if D_+ is a function of w_+ alone and D_- is a function of w_- alone, that is if the field components are analytic or anti-analytic functions. For such fields, there is no conical refraction, and (for example) a pattern of zeros in the incident field propagates not conically but as a set of straight optical vortex lines parallel to the ζ direction. However, these analytic functions do not represent realistic optical beams, which must decay in all directions ϕ as $\rho \to \infty$.

References

Belsky, A.M., Khapalyuk, A.P., 1978, Internal conical refraction of bounded light beams in biaxial crystals, Opt. Spectrosc. (USSR) **44**, 436–439.

Belsky, A.M., Stepanov, M.A., 1999, Internal conical refraction of coherent light beams, Opt. Commun. **167**, 1–5.

Belsky, A.M., Stepanov, M.A., 2002, Internal conical refraction of light beams in biaxial gyrotropic crystals, Opt. Commun. **204**, 1–6.

Berry, M.V., 1983, Semiclassical Mechanics of regular and irregular motion, in: Iooss, G., Helleman, R.H.G., Stora, R. (Eds.), Les Houches Lecture Series, vol. **36**, North-Holland, Amsterdam, pp. 171–271.

Berry, M.V., 1984, Quantal phase factors accompanying adiabatic changes, Proc. Roy. Soc. Lond. A **392**, 45–57.

Berry, M.V., 2001, Geometry of phase and polarization singularities, illustrated by edge diffraction and the tides, in: Soskin, M. (Ed.), Singular Optics 2000, vol. **4403**, SPIE, Alushta, Crimea, pp. 1–12.

Berry, M.V., 2004a, Asymptotic dominance by subdominant exponentials, Proc. Roy. Soc. A **460**, 2629–2636.

Berry, M.V., 2004b, Conical diffraction asymptotics: fine structure of Poggendorff rings and axial spike, J. Optics A **6**, 289–300.

Berry, M.V., 2004c, Physics of nonhermitian degeneracies, Czech. J. Phys. **54**, 1040–1047.

Berry, M.V., Dennis, M.R., 2003, The optical singularities of birefringent dichroic chiral crystals, Proc. Roy. Soc. A **459**, 1261–1292.

Berry, M.V., Dennis, M.R., Lee, R.L.J., 2004, Polarization singularities in the clear sky, New J. of Phys. **6**, 162.

Berry, M.V., Jeffrey, M.R., 2006a, Chiral conical diffraction, J. Opt. A **8**, 363–372.

Berry, M.V., Jeffrey, M.R., 2006b, Conical diffraction complexified: dichroism and the transition to double refraction, J. Opt. A **8**, 1043–1051.

Berry, M.V., Jeffrey, M.R., Lunney, J.G., 2006, Conical diffraction: observations and theory, Proc. R. Soc. A **462**, 1629–1642.

Berry, M.V., Jeffrey, M.R., Mansuripur, M., 2005, Orbital and spin angular momentum in conical diffraction, J. Optics A **7**, 685–690.

Berry, M.V., Wilkinson, M., 1984, Diabolical points in the spectra of triangles, Proc. Roy. Soc. Lond. A **392**, 15–43.

Born, M., Wolf, E., 1999, Principles of Optics, seventh ed., Pergamon, London.

Cederbaum, L.S., Friedman, R.S., Ryaboy, V.M., Moiseyev, N., 2003, Conical intersections and bound molecular states embedded in the continuum, Phys. Rev. Lett. **90**, 013001-1-4.

Chu, S.Y., Rasmussen, J.O., Stoyer, M.A., Canto, L.F., Donangelo, R., Ring, P., 1995, Form factors for two-neutron transfer in the diabolical region of rotating nuclei, Phys. Rev. C **52**, 685–696.

Deschamps, G.A., 1971, Gaussian beam as a bundle of complex rays, Electronics Lett. **7**, 684–685.

Ferretti, A., Lami, A., Villani, G., 1999, Transition probability due to a conical intersection: on the role of the initial conditions of the geometric setup of the crossing surfaces, J. Chem. Phys. **111**, 916–922.

Fève, J.P., Boulanger, B., Marnier, G., 1994, Experimental study of internal and external conical refraction in KTP, Opt. Commun. **105**, 243–252.

Graves, R.P., 1882, Life of Sir William Rowan Hamilton, vol. **1**, Hodges Figgis, Dublin.

Hamilton, W.R., 1837, Third Supplement to an Essay on the Theory of Systems of Rays, Trans. Royal Irish Acad. **17**, 1–144.

Herzberg, G., Longuet-Higgins, H.C., 1963, Intersection of potential-energy surfaces in polyatomic molecules, Disc. Far. Soc. **35**, 77–82.

Indik, R.A., Newell, A.C., 2006, Conical refraction and nonlinearity, Optics Express **14**, 10614–10620.
Jeffrey, M.R., 2007, The spun cusp complexified: complex ray focusing in chiral conical diffraction, J. Opt. A. **9**, 634–641.
King, T.A., Hogervorst, W., Kazak, N.S., Khilo, N.A., Ryzhevich, A.A., 2001, Formation of higher-order Bessel light beams in biaxial crystals, Opt. Commun. **187**, 407–414.
Lalor, E., 1972, An analytical approach to the theory of internal conical refraction, J. Math. Phys. **13**, 449–454.
Landau, L.D., Lifshitz, E.M., Pitaevskii, L.P., 1984, Electrodynamics of Continuous Media, Pergamon, Oxford.
Liebisch, T., 1896, Grundriss der Physikalischen Krystallographie, Von Veit & Comp, Leipzig.
Lloyd, H., 1837, On the phenomena presented by light in its passage along the axes of biaxial crystals, Trans. R. Ir. Acad. **17**, 145–158.
Ludwig, D., 1961, Conical refraction in crystal optics and hydromagnetics, Comm. Pure. App. Math. **14**, 113–124.
Lunney, J.G., Weaire, D., 2006, The ins and outs of conical refraction, Europhysics News **37**, 26–29.
Mead, C.A., Truhlar, D.G., 1979, On the determination of Born–Oppenheimer nuclear motion wave functions including complications due to conical intersections and identical nuclei, J. Chem. Phys. **70**, 2284–2296.
Mikhailychenko, Y.P., 2005, Large scale demonstrations on conical refraction, http://www.demophys.tsu.ru/Original/Hamilton/Hamilton.html.
Naida, O.N., 1979, "Tangential" conical refraction in a three-dimensional inhomogeneous weakly anisotropic medium, Sov. Phys. JETP **50**, 239–245.
Nussenzveig, H.M., 1992, Diffraction Effects in Semiclassical Scattering, University Press, Cambridge.
Nye, J.F., 1999, Natural Focusing and Fine Structure of Light: Caustics and Wave Dislocations, Institute of Physics Publishing, Bristol.
O'Hara, J.G., 1982, The prediction and discovery of conical refraction by William Rowan Hamilton and Humphrey Lloyd (1832–1833), Proc. R. Ir. Acad. **82A**, 231–257.
Perkal'skis, B.S., Mikhailychenko, Y.P., 1979, Demonstration of conical refraction, Izv. Vyss. Uch. Zav. Fiz. **8**, 103–105.
Poggendorff, J.C., 1839, Ueber die konische Refraction, Pogg. Ann. **48**, 461–462.
Potter, R., 1841, An examination of the phaenomena of conical refraction in biaxial crystals, Phil. Mag. **8**, 343–353.
Raman, C.V., 1941, Conical refraction in naphthalene crystals, Nature **147**, 268.
Raman, C.V., Rajagopalan, V.S., Nedungadi, T.M.K., 1941, Conical refraction in naphthalene crystals, Proc. Ind. Acad. Sci. A **14**, 221–227.
Schell, A.J., Bloembergen, N., 1977, Second harmonic conical refraction, Opt. Commun. **21**, 150–153.
Schell, A.J., Bloembergen, N., 1978a, Laser studies of internal conical diffraction. I. Quantitative comparison of experimental and theoretical conical intensity dirstribution in aragonite, J. Opt. Soc. Amer. **68**, 1093–1098.
Schell, A.J., Bloembergen, N., 1978b, Laser studies of internal conical diffraction. II. Intensity patterns in an optically active crystal, α-iodic acid, J. Opt. Soc. Amer. **68**, 1098–1106.
Shih, H., Bloembergen, N., 1969, Conical refraction in second harmonic generation, Phys. Rev. **184**, 895–904.
Silverman, M., 1980, The curious problem of spinor rotation, Eur. J. Phys. **1**, 116–123.
Soskin, M.S., Vasnetsov, M.V., 2001, Singular optics, in: Progress in Optics, vol. **42**, North-Holland, Amsterdam, pp. 219–276.
Stepanov, M.A., 2002, Transformation of Bessel beams under internal conical refraction, Opt. Commun. **212**, 11–16.

Uhlenbeck, K., 1976, Generic properties of eigenfunctions, Am. J. Math. **98**, 1059–1078.
Uhlmann, A., 1982, Light intensity distribution in conical refraction, Commn. Pure. App. Math. **35**, 69–80.
van de Hulst, H.C., 1981, Light Scattering by Small Particles, Dover, New York.
VCT, 2006, Home page of Vision Crystal Technology, http://www.vct-ag.com/.
Voigt, W., 1905a, Bemerkung zur Theorie der konischen Refraktion, Phys. Z. **6**, 672–673.
Voigt, W., 1905b, Theoretisches unt Experimentelles zur Aufklärung des optisches Verhaltens aktiver Kristalle, Ann. Phys. **18**, 645–694.
Von Neumann, J., Wigner, E., 1929, On the behavior of eigenvalues in adiabatic processes, Phys. Z. **30**, 467–470.
Warnick, K.F., Arnold, D.V., 1997, Secondary dark rings of internal conical refraction, Phys. Rev. E **55**, 6092–6096.
Wolfram, S., 1996, The Mathematica Book, University Press, Cambridge.